Journal of Nuclear Medicine, published on August 27, 2015 as doi:10.2967/jnumed.115.158121

Mapping radiation injury and recovery in bone marrow using ^{18}F-FLT PET/CT and USPIO-MR imaging in a rat model

David A. Rendon[1*], Khushali Kotedia[1*], Solmaz F. Afshar[2], Jyotinder N. Punia[3], Omaima M. Sabek[2], Beverly A. Shirkey[4], Janice A. Zawaski[1], and M. Waleed Gaber[1**]

[1]Hematology-Oncology Section, Department of Pediatrics, Baylor College of Medicine, Houston, TX

[2]Department of Surgery, Houston Methodist Hospital Research Institute, Houston, TX

[3]Department of Pathology and Immunology, Baylor College of Medicine, Houston, TX

[4]Center for Outcomes Research, Department of Surgery, Houston Methodist Hospital Research Institute, Houston, TX

*These two authors contributed equally to this work.

**Corresponding author to whom correspondence should be directed.

Corresponding Author:

M. Waleed Gaber, PhD

Associate Professor

Baylor College of Medicine, Hematology-Oncology Section, Department of Pediatrics

1102 Bates Street, Suite 200.04

Houston, TX 77030

Tel: +1 (832) 824 3170

Fax: +1 (832) 825 4039

E-mail: gaber@bcm.edu

First Authors:

David A. Rendon, PhD

Clinical Instructor

Baylor College of Medicine, Hematology-Oncology Section, Department of Pediatrics

1102 Bates Street, Suite 200.07

Houston, TX 77030

Tel: +1 (832) 824 3

Fax: +1 (832) 825 4039

E-mail: darendon@txch.org

Khushali Kotedia, PhD

Postdoctoral Fellow

Baylor College of Medicine, Hematology-Oncology Section, Department of Pediatrics

1102 Bates Street, Suite 200.07

Houston, TX 77030

Tel: +1 (832) 824 0243

Fax: +1 (832) 825 4039

E-mail: kxkotedi@txch.org

Word Count: 4986

Running Title: Imaging radiation-induced marrow injury

ABSTRACT

We present and test the use of multimodality imaging as a topological tool to map the amount of the body exposed to ionizing radiation and the location of exposure, which are important indicators of survival and recovery. To achieve our goal, PET/CT imaging utilizing 3'-deoxy-3'-^{18}F-fluorothymidine (^{18}F-FLT) was used to measure cellular proliferation in bone marrow (BM), while MR imaging using ultra-small superparamagnetic iron oxide (USPIO) particles provided noninvasive information on radiation-induced vascular damage.

Methods: Animals were x-ray irradiated at a dose of 7.5 Gy with one of three radiation schemes: whole body irradiation (WBI), half body shielding (HBS), or one leg shielding (1LS), and were imaged repeatedly. The spatial information from the CT scan was used to segment the region corresponding to BM from the PET scan using algorithms developed in-house, allowing for quantification of proliferating cells, and BM blood volume was estimated by measuring the changes in the T_2 relaxation rates (ΔR_2) collected from MR scans.

Results: ^{18}F-FLT PET/CT imaging differentiated irradiated from unirradiated BM regions. Two days post irradiation, proliferation of 1LS animals was significantly lower than sham ($p = 0.0001$ femurs; $p < 0.0001$ tibias) and returned to sham levels by day 10 ($p = 0.6344$ femurs; $p = 0.3962$ tibias). The degree of shielding affected proliferation recovery, showing an increase ($p = 0.0310$ femurs; $p = 0.5832$ tibias) in the irradiated BM of HBS animals when compared to 1LS. MR imaging of irradiated spines detected

radiation-induced BM vascular damage, measured by the significant increase in ΔR_2 two days after WBI ($p = 0.0022$) and HBS ($p = 0.0003$) with a decreasing trend of values, returning to levels close to baseline over 10 days. Our data was corroborated using gamma counting and histopathology.

Conclusions: We demonstrated that ^{18}F-FLT PET/CT and USPIO-MRI are valuable tools in mapping regional radiation exposure and the effects of radiation on BM. Analysis of the FLT signal allowed for a clear demarcation of exposed BM regions and elucidated the kinetics of BM recovery, while USPIO-MRI was used to assess vascular damage and recovery.

Key Words: radiation, bone marrow, proliferation, ^{18}F-FLT PET/CT, USPIO-MRI

INTRODUCTION

In the aftermath of a nuclear disaster, a victim's total dose and degree of radiation exposure will be a complicated function of their distance from the source of radiation and the presence of shielding factors in direct line to that source (*1*). The severity of radiation injury depends in part on the total dose absorbed, amount of the body that is exposed, and the anatomical region that has been irradiated. The extent of radiation exposure will result in marked differences in the victim's survival probability, their medical management, and in their acute and late prognosis, necessitating long-term monitoring of all survivors, with some requiring immediate medical attention (*2*). Furthermore, in radiotherapy for cancer patients, BM toxicity can be a limiting factor in determining therapeutic radiation doses. Although medical imaging is at the forefront of early diagnosis of disease and patient triaging, imaging is not yet an integrated tool in emergency preparedness plans in response to a nuclear disaster (*3*). In this paper, we address this issue by making use of 3'-deoxy-3'-^{18}F-fluorothymidine (^{18}F-FLT) PET/CT and ultra-small superparamagnetic iron oxide (USPIO)-MR imaging in a rat model of whole and partial body radiation exposure to measure bone marrow (BM) proliferation and vascular damage as surrogates for mapping the amount of body exposed and the anatomical region irradiated.

BM occupies interstices within the bones distributed throughout the entire skeleton, and is one of the most proliferative and radiosensitive organs in the body, with a highly vascularized network of thin-walled, fenestrated sinusoidal endothelial cells (*4*).

This microvasculature, forming the blood-bone marrow barrier (BMB), serves as a gatekeeper regulating the passage of hematopoietic cells between the marrow and the circulation, and is susceptible to the effects of radiation, displaying signs of necrosis, marked dilation, and damage, with plasma and red blood cell leakage into the BM parenchyma (*5*). Whole body irradiation is used as a conditioning regimen for BM transplantation by disrupting the BMB, facilitating the passage of transplanted cells, and suppressing their rejection through its myeloablation effects.

^{18}F-FLT is a thymidine analogue that is phosphorylated by thymidine kinase 1 during DNA synthesis, becoming trapped within the cell (*6*). Accumulation of FLT is greater in proliferating tissues, making it ideal for its utilization in imaging BM and the effect of irradiation on its proliferation (*7*). USPIOs have a long blood half-life (*8*) and they alter the T_2 relaxation, causing a signal loss between normal and damaged tissue which can be caused by an increase in blood volume, such as what occurs in the radiation-induced disruption of BMB integrity, resulting in the extravasation of the particles into the parenchyma.

In this work, we use a rat model with various degrees of radiation exposure to demonstrate the feasibility of our paradigm by making use of ^{18}F-FLT, a proliferation molecular agent, and USPIO, a magnetic contrast agent, to measure radiation-induced BM eradication and BMB disruption, its topological location, and kinetics of recovery.

MATERIALS AND METHODS

Animal Irradiation

All animal experiments were performed in accordance with the regulations of the Institutional Animal Care and Use Committee at Baylor College of Medicine. For the PET/CT studies, 5-6 week-old male Sprague-Dawley rats (Harlan Laboratories) were divided into four groups: a control group that received no radiation (sham, whole body irradiated (WBI, half body shielded (HBS), or one leg shielded (1LS). To ensure MR field homogeneity, small-sized male Fischer 344 rats (Harlan Laboratories) aged 6-7 weeks were used for the MR studies, and were either WBI or HBS. All animals were anesthetized with isoflurane (2%) in oxygen, positioned prone, and x-ray irradiated 7.5 Gy (RS 2000 x-ray irradiator) at a dose rate of 1.16 Gy/min. Shielding was accomplished using 0.5 cm-thick slabs of malleable lead covering the entire leg or half of the animal's body of 1LS or HBS animals, respectively.

^{18}F-FLT PET/CT Imaging

CT and PET scans were performed using an Inveon scanner (Siemens AG). Due to imaging-field limitations of the scanner in obtaining full-body scans of a rat, the scans were divided into two sessions: the first covering the upper part of the body to the mid-abdomen, and the second covering the lower part. Before scanning, each animal was injected intravenously with 1.3 units/g thymidine phosphorylase (TP) (Sigma-Aldrich Co), to reduce the serum levels of endogenous thymidine (*9*). Forty-five minutes post TP injection, the rat was injected IV with 12.58 MBq (340 μCi) of ^{18}F-FLT (Cyclotope). Rats were anesthetized with 2% isoflurane in oxygen, adjusted to maintain a rate of 30-40 breaths/minute, and placed prone inside a half-cut plastic bottle (Ozarka, Nestlé Waters North America, Inc.) to allow for manipulation of the animal while

maintaining its position, with a respiration pad (BioVet) to monitor the animal continuously. First, a CT scan was acquired using the following protocol: two bed positions, each of which containing 220 acquired projections covering 220°, with a source-to-detector distance of 312.91 mm and a source-to-center of rotation distance of 183.92 mm. The x-ray tube voltage and current were set at 80 kVp and 500 μA, respectively, with an exposure time of 650 ms per projection. The animal was imaged for 20 minutes starting one hour after injection of ^{18}F-FLT. The bottle was then rotated 180° to scan the lower part of the body using the same protocol as described above. The scans were positioned to have an overlap to help produce a complete rat body scan. The spatial information from the CT scan was used to segment the region corresponding to BM from the PET scan using algorithms developed in-house (Supplemental Video 1), as described in the supplement.

Gamma Counter Measurements

Cell proliferation measurements using ^{18}F-FLT PET/CT were corroborated using a gamma counter (Wizard^2 2480, PerkinElmer). Animal experiments followed the same protocol as previously described for injections of TP and ^{18}F-FLT. To standardize the time allowed for FLT uptake, tissue-harvesting times reproduced the same time frame used in the PET/CT imaging studies. The legs of the animal were isolated and the FLT radioactivity in the femurs, tibias, and blood were counted, corrected for the radionuclide decay to the time of injection, and normalized to the injected dose and weight of the tissue.

In Vivo MR Imaging

MR images were acquired using a Bruker Biospec 94/30 operating at 9.6 T and equipped with a 200 mT/m gradient coil insert. A 72 mm linear birdcage resonator was used for radiofrequency transmission and a 2 cm diameter surface coil, used in the receive-only mode, was placed on the lateral surface of the spine covering vertebrae T11-L1. MR images were acquired using Bruker's PARAVISION 5.1 software. A respiratory sensor pillow (SA Instruments) was placed on the abdomen of the animals to gate each spin-echo to the same position in the respiratory cycle and to monitor the respiration rate. Respiration of the animal was maintained at 30 breaths/minute by a mixture of 2% isoflurane in oxygen. Body temperature was maintained at 37^{o}C by a re-circulating water system incorporated in the animal bed. The animals were placed prone in the scanner with the head stabilized by a teeth holder and secured to the cradle. A T_2-weighted rapid acquisition with relaxation enhancement (RARE) sequence was used to acquire sagittal anatomical images using the following parameters: TR/TE = 2000/17.6 ms, RARE factor = 4, slice thickness = 0.8 mm, slices = 3, number of excitations = 6, matrix dimensions = 256 x 256 and field-of-view = 3 x 3 cm, giving an in-plane resolution of 117 x 117 μm^2. Following localizer acquisitions, four axial slices through the bone marrow were selected for susceptibility contrast MR imaging (Supplemental Fig. 1). To measure the change in relaxation rate, ΔR_2, as described by Boxerman et. al., (*10*) a T_2-weighted RARE sequence was performed before and after administration of 4 mg Fe/kg Ferumoxytol (Feraheme®, AMAG Pharmaceuticals Inc.) IV, via a lateral tail vein catheter, using the parameters: TR/TE = 2000/20.41 ms, RARE factor = 4, slice thickness = 1.5 mm, matrix

size = 128 x 128, 2 averages, field-of-view = 1.2 x 1.2 cm, giving an in-plane resolution of 94 x 94 μm^2. ΔR_2 color-coded relative blood volume maps were calculated using customized scripts in MatLab, as described in the supplement.

Histopathological Analysis

BM specimens were fixed in 10% buffered formalin for 48 hours and decalcified (TBD-2 Decalcifier, Thermo Scientific) for 72 hours. Paraffin embedded tissue was cut in 4 μm sections, and stained with one of three stains: hematoxylin and eosin (H&E), Factor VIII (FVIII), an immunohistochemical stain marking endothelial cells, megakaryocytes and platelets, or with bromodeoxyuridine, a thymidine analogue used to label cells in the S-phase of DNA synthesis, injected 4 hours prior to euthanization. BM smears were also collected for Prussian blue staining to detect the presence of iron.

Statistical Analysis

Data were presented as means and standard deviation of the means. Group means were compared using a Student's t-test. When comparing irradiated to sham legs, paired t-tests were used, assuming unequal variances. A linear model adjusting for the repeated measures on each animal was used to analyze the MR data. Statistical significance was assigned for $P < 0.05$. All statistical computations were processed using Stata 13.1 for Windows (StataCorp LP).

RESULTS

Proliferation

^{18}F-FLT PET/CT Imaging. Imaging can differentiate irradiated from unirradiated

bone marrow regions throughout the body (Fig. 1). The backbone (total standard uptake value (SUV) = 24.86%) contained the largest amount of proliferating BM, followed by the lower and upper limbs, while the femur had the highest proliferation per unit volume (Table 1). Our PET data demonstrated a clear effect of radiation exposure on BM proliferation (Fig. 2). Measured by SUV, proliferation was significantly lower in the irradiated femurs of the 1LS group ($p = 0.0001$) two days post irradiation (0.51 ± 0.076, $n = 6$) compared to sham (1.52 ± 0.247, $n = 6$) (Fig. 2A). Similarly, proliferation was significantly lower ($p < 0.0001$) in the irradiated tibias of the 1LS group (0.49 ± 0.133, $n = 8$) when compared to sham (1.14 ± 0.181, $n = 6$), (Fig. 2B). Ten days post exposure, proliferation was restored to control levels whereby both the irradiated femurs and tibias of the 1LS group (1.44 ± 0.362, and 1.26 ± 0.301, $n = 8$, respectively) were statistically equal to their sham equivalent ($p = 0.6344$, and $p = 0.3962$, respectively). Considering the effects of the degree of shielding on recovery by day 10, the irradiated tibias from the 1LS group were not significantly different ($p = 0.5832$) from the irradiated tibias of the HBS group (1.32 ± 0.081, $n = 4$), possibly due to the minimal amount of BM in the tissue. However, the irradiated femurs of the 1LS group differed significantly ($p = 0.0310$) from the irradiated femurs of the HBS group (1.81 ± 0.145, $n = 4$), suggesting a significant dependence in recovery of BM proliferation on the amount of BM exposed, with greater robustness as the amount of shielded BM increased.

Gamma Counting. As in the PET data, the accumulation of ^{18}F-FLT in sham blood, femurs and tibias (0.00091 ± 0.000078, 0.00897 ± 0.001596 and $0.00653 \pm$

0.001047 %ID/g, respectively) was significantly different ($p < 0.0001$) from that of irradiated blood, femurs and tibias of 1LS animals (0.00072 ± 0.000163, 0.00112 ± 0.000406 and 0.00098 ± 0.000389 %ID/g, respectively) two days post radiation exposure.

Histopathology. To further corroborate our findings with other measures of proliferation, we stained femur sections with H&E (Fig. 3, Supplemental Fig. 2) and bromodeoxyuridine (Supplemental Fig. 3) at two and ten days post irradiation. Sham tissue showed structured, cellularly dense, and highly proliferative BM, while at two days post radiation exposure, the BM showed a subtotal loss of hematopoietic cells, massive hemorrhaging, a loss of structure with no osteoblasts bordering the marrow along the bone, and a drastic loss in proliferation, similar to what is observed in our ^{18}F-FLT studies. Although at ten days post exposure the BM showed signs of regaining its organized structure and revitalization in proliferation, there are indications of persistent damage evidenced by the presence of adipose tissue.

Vascularity

MR Imaging. A heat mask generated at various time points post radiation exposure (Supplemental Fig. 4) showed a visual map of the changes in the relaxation rate, ΔR_2, following injury and up to ten days thereafter. Using linear regression analysis we observed that within a particular experimental group (WBI and HBS), ΔR_2 (S^{-1}) changed significantly over time. Two days post WBI (38.69 ± 7.65) there was a significant increase ($p = 0.0004$) in ΔR_2 (Fig. 4) when compared to baseline (17.38 ± 3.03), and remained significant at day 5 (26.50 ± 7.79, $p=0.0479$), with a gradual decrease back to nonsignificant values by day 7 (13.47 ± 5.25, $p=0.7693$) and day 10 (11.03 ± 3.70,

p=0.5473). To test whether BM shielding had any positive effect on vascular damage, we shielded half of the animals' body and measured vascular changes in the same irradiated vertebral region. Two days post HBS (37.17 ± 1.95, there was a significant increase (p <0.0001) in ΔR_2 (Fig. 4) when compared to baseline (10.31 ± 4.31), and stayed significant at day 5 (21.38 ± 4.81, p=0.0220) with a gradual decrease back to values insignificant from sham by day 7 (11.42 ± 4.73, p=0.0852), but dipping significantly below sham at day 10 (8.48 ± 3.85, p=0.0118). Adjusting for repeated measures within the rats and time points, the average effect of WBI versus HBS was an increase of 3.7.

Histopathology. The H&E-stained sections of sham vertebrae (Fig. 5A top) showed normal BM architecture. The background stroma showed small, intact caliber blood vessels, highlighted by a positive brown hue in the immunohistochemical stain for FVIII (Fig. 5A bottom). Two days following WBI exposure (Fig. 5B), there was markedly hypocellular marrow with prominent stromal damage, including extravasation of red blood cells and dilated and disrupted blood vessels. Seven days following exposure (Fig. 5C), there was still markedly hypocellular marrow while adipose tissue increased to fill the marrow space, with extravasated red blood cells still present and hematopoietic cells almost absent. This same trend persisted for ten days, where BM remained markedly hypocellular and the marrow replaced by adipose tissue (Fig. 5D). However by this time, the stroma appeared to be recovering; scant extravasated red blood cells, no large irregular blood vessels, and rare small aggregates of hematopoietic cells were seen. We scored these H&E sections (Table 2) and found that the highest score for hemorrhage was at two days post exposure. Two days following HBS, the exposed vertebral sections

demonstrated the same features as WBI BM (Supplemental Fig. 5A) with extravasated iron particles as shown in the Prussian blue-stained BM smears (Supplemental Fig. 6). However at day ten, the BM showed signs of recovery with a significant number of hematopoietic cells and vascular reconstruction (Supplemental Fig. 5, 6C).

DISCUSSION

Our results demonstrated that imaging not only can differentiate irradiated from unirradiated BM regions, but can also measure BM recovery. ^{18}F-FLT PET/CT imaging can map the degree and location of radiation exposure, while USPIO-MR imaging can be used to measure radiation-induced vascular damage. We also observed that the amount of BM proliferation, but not vascular recovery, in irradiated regions is significantly dependent on the degree of body exposed. Using gamma counting measurements, we verified that the signal obtained from the PET scans of BM is independent of our imaging procedures. Immunohistochemical staining demonstrated that proliferation was affected by radiation exposure in a manner similar to our ^{18}F-FLT measurements, as was vascular integrity, determined from our MR data.

^{18}F-FLT PET/CT imaging demonstrated a radiation-induced reduction in proliferation at two days post exposure (Fig. 2), and was restored to near-control levels by day ten. This observation was confirmed histologically using H&E staining as a measure of progenitor cell density (Fig. 3, Supplemental Fig. 2), and bromodeoxyuridine staining of proliferative cells (Supplemental Fig. 3). In our analysis, we distinguished equal volumes of active BM from different bones, and further, from different regions

within the bone. From our measurements, we derived two distinct values that provided information about the BM in the region of interest: (a) an average activity (average SUV) which indicated the average rate of proliferation throughout the volume and (b) the integration of that average activity (total SUV) which specified the total proliferation. The first value was indicative of the degree of participation and demand for proliferating BM cells in hematopoiesis, while the second value represented the total amount of proliferating cells in a given region. The sternum was a prime example of how these two measurements provided us with additional information on BM activity: its average SUV was one of the highest, but due to its small volume it contributed less than 2% of the total SUV of the body. From the total SUV, we determined that most of the BM activity was concentrated in the backbone, femurs, skull, and tibias (Table 1), agreeing with Shaposhnikov et, al. (*11*) who reported that the highest cell counts from bone marrow biopsies were found, in descending order, in the backbone, skull, pelvis, femur, and tibia. Together, the average and total SUV can be utilized in a victim's triaging in the event of a nuclear disaster, and when making decisions on the use of radiation therapy and/or cytotoxic drugs in the treatment planning of malignant diseases (*12*).

Our results are also partially consistent with previous works that directly measure the distribution of BM in humans, with the major discrepancy being the percent of BM in the limbs. Ellis et. al., (*13*) measured a relatively low amount of red BM in the proximal ends of the femur and humerus with negligible amounts in the rest of the limbs, while we observed that the femurs and tibias contain a quarter of BM activity in unirradiated rats (13.7% and 11.7%, respectively), as well as an appreciable activity in the arms. Aside

from the obvious difference in species, this discrepancy can be explained by the age of these adolescent rats, in comparison to the human data which was taken from adult subjects, as red BM recedes with age (*14*).

Radiation exposure not only reduces the progenitor cell population and its proliferative activity, but it also damages the BMB and the sinusoidal architecture necessary for the continued production and delivery of hematopoietic cells (*4*). Our USPIO-MRI data, confirmed by immunohistochemical staining (Fig. 5), shows a clear indication of radiation induced vascular hemorrhage (H&E) and a loss of vascular integrity (Factor VIII) with a peak at two days following exposure that subsides by day ten. Note that the kinetics of vascular response in both the imaging and histological data coincides, demonstrating the ability of USPIO-MRI to measure radiation-induced vascular disruption. Further, the disruption did not differ significantly between radiation schemes two days post exposure (Fig. 5 and Supplemental Fig. 5). Philippens et, al. have demonstrated the presence of USPIO particles in the irradiated rat spinal cord using Prussian blue staining and the corresponding MRI signal intensity changes induced by its presence (*15*). Daldrup et, al. (*16*) used electron microscopy to detect USPIO particles in the BM, and in a different study they show that the MR dynamic signal increased significantly 1–2 days after total body irradiation, which is consistent with our data (*17*). Further, Fliender et, al. (*4*) and others have reported that revascularization of BM after irradiation is necessary for hematopoietic regeneration, as also supported by our data, which showed that vascular recovery coincided with increased hematopoiesis.

One main concern in the use of PET/CT imaging is the perceived damaging

effect of exposing radiation victims to further radiation. However, the accuracy and sensitivity that such imaging exams provide would outweigh these risks, given the comparatively small dose of ^{18}F-based radiopharmaceuticals needed for PET imaging (*12*). Additionally, CT scans associated with PET studies are intended only for PET attenuation correction and anatomical localization of the activity of the radiotracer, whose doses are usually estimated to be only two thirds or less of the doses delivered by the PET scan (*18*).

CONCLUSION

Our goal was to investigate the possibility of utilizing medical imaging techniques to design and implement a triaging system that can be employed in a nuclear incident or accidental exposure. We presented data that demonstrated the use of imaging to delineate the radiation-exposed regions of BM and the effect of shielding on its recovery. Our goal was achieved using ^{18}F-FLT PET/CT to record changes in proliferation and the utility of USPIO-MRI in monitoring vascular changes. These tools can be used to distinguish the extent of bodily exposure and in the long-term management of radiation victims and radiotherapy patients.

ACKNOWLEDGMENTS

This work was supported in part by a grant from the Defense Threat Reduction Agency [HDTRA 1-10-1-0026]. The authors would like to thank Texas Children's Hospital for the use of the Small Animal Imaging facility.

REFERENCES

1. Knebel AR, Coleman CN, Cliffer KD, et al. Allocation of scarce resources after a nuclear detonation: setting the context. *Disaster Med Public Health Prep.* Mar 2011;5 Suppl 1:S20-31.
2. Dorr HD, Meineke V. Appropriate radiation accident medical management: necessity of extensive preparatory planning. *Radiat Environ Biophys.* Nov 2006;45(4):237-244.
3. Murrain-Hill P, Coleman CN, Hick JL, et al. Medical response to a nuclear detonation: creating a playbook for state and local planners and responders. *Disaster Med Public Health Prep.* Mar 2011;5 Suppl 1:S89-97.
4. Fliedner TM, Graessle D, Paulsen C, Reimers K. Structure and function of bone marrow hemopoiesis: mechanisms of response to ionizing radiation exposure. *Cancer Biother Radiopharm.* Aug 2002;17(4):405-426.
5. Kopp HG, Avecilla ST, Hooper AT, Rafii S. The bone marrow vascular niche: home of HSC differentiation and mobilization. *Physiology (Bethesda).* Oct 2005;20:349-356.
6. Rasey JS, Grierson JR, Wiens LW, Kolb PD, Schwartz JL. Validation of FLT uptake as a measure of thymidine kinase-1 activity in A549 carcinoma cells. *J Nucl Med.* Sep 2002;43(9):1210-1217.

7. Agool A, Slart RH, Thorp KK, et al. Effect of radiotherapy and chemotherapy on bone marrow activity: a 18F-FLT-PET study. *Nucl Med Commun.* Jan 2011;32(1):17-22.

8. Weissleder R, Elizondo G, Wittenberg J, Rabito CA, Bengele HH, Josephson L. Ultrasmall superparamagnetic iron oxide: characterization of a new class of contrast agents for MR imaging. *Radiology.* May 1990;175(2):489-493.

9. van Waarde A, Cobben DC, Suurmeijer AJ, et al. Selectivity of 18F-FLT and 18F-FDG for differentiating tumor from inflammation in a rodent model. *J Nucl Med.* Apr 2004;45(4):695-700.

10. Boxerman JL, Hamberg LM, Rosen BR, Weisskoff RM. MR contrast due to intravascular magnetic susceptibility perturbations. *Magn Reson Med.* Oct 1995;34(4):555-566.

11. Shaposhnikov VL. [Distribution of the bone marrow cells in the skeleton of mice]. *Biull Eksp Biol Med.* May 1979;87(5):483-485.

12. McGuire SM, Menda Y, Boles Ponto LL, Gross B, Buatti J, Bayouth JE. 3'-deoxy-3'-[(1)(8)F]fluorothymidine PET quantification of bone marrow response to radiation dose. *Int J Radiat Oncol Biol Phys.* Nov 1 2011;81(3):888-893.

13. Ellis RE. The distribution of active bone marrow in the adult. *Phys Med Biol.* Jan 1961;5:255-258.

14. Mauch P, Botnick LE, Hannon EC, Obbagy J, Hellman S. Decline in bone marrow proliferative capacity as a function of age. *Blood.* Jul 1982;60(1):245-252.

15. Philippens ME, Gambarota G, Pikkemaat JA, Peeters WJ, van der Kogel AJ, Heerschap A. Characterization of late radiation effects in the rat thoracolumbar spinal cord by MR imaging using USPIO. *Magma.* Dec 2004;17(3-6):303-312.

16. Daldrup HE, Link TM, Blasius S, et al. Monitoring radiation-induced changes in bone marrow histopathology with ultra-small superparamagnetic iron oxide (USPIO)-enhanced MRI. *J Magn Reson Imaging.* May 1999;9(5):643-652.

17. Daldrup-Link HE, Link TM, Rummeny EJ, et al. Assessing permeability alterations of the blood-bone marrow barrier due to total body irradiation: in vivo quantification with contrast enhanced magnetic resonance imaging. *Bone Marrow Transplant.* Jan 2000;25(1):71-78.

18. Gahramanov S, Muldoon LL, Varallyay CG, et al. Pseudoprogression of glioblastoma after chemo- and radiation therapy: diagnosis by using dynamic susceptibility-weighted contrast-enhanced perfusion MR imaging with ferumoxytol versus gadoteridol and correlation with survival. *Radiology.* Mar 2013;266(3):842-852.

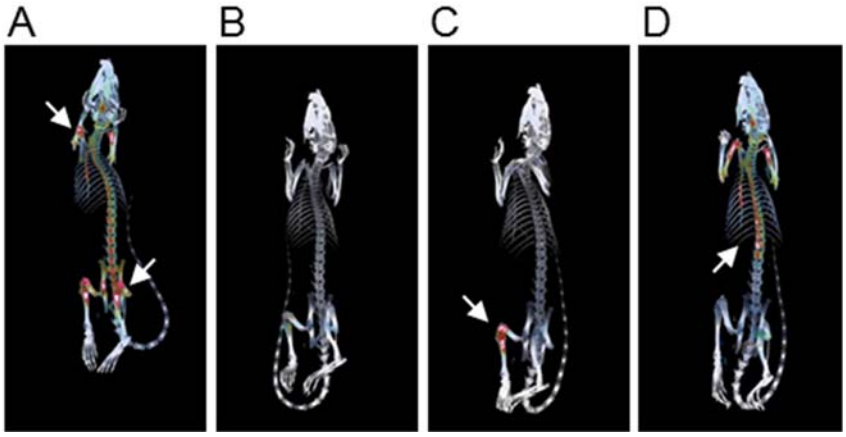

FIGURE 1. ^{18}F-FLT PET/CT imaging maps the degree and location of radiation exposure. Reconstructed PET/CT images showing sites of radiation injury in a rat with (A) sham irradiation (B) whole body irradiation (C) one leg shielding and (D) half body shielding. Arrows point to hot spots where ^{18}F-FLT was uptaken.

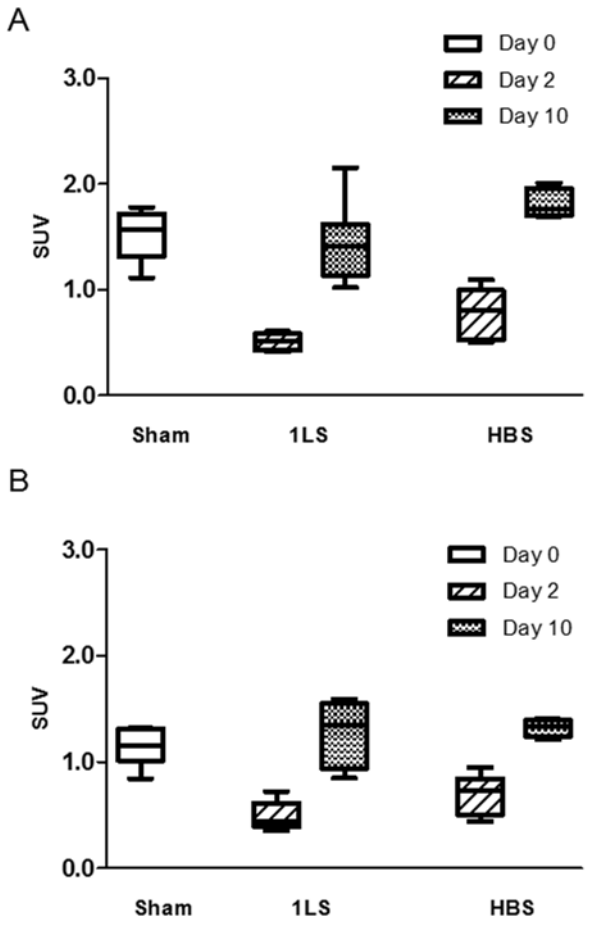

FIGURE 2. ^{18}F-FLT PET/CT data demonstrates a clear effect of radiation exposure on BM proliferation. Box plot of average standard uptake value (SUV) of irradiated (A) femur and (B) tibia at 2 and 10 days post from left to right: sham, one leg shielding, and half body shielding.

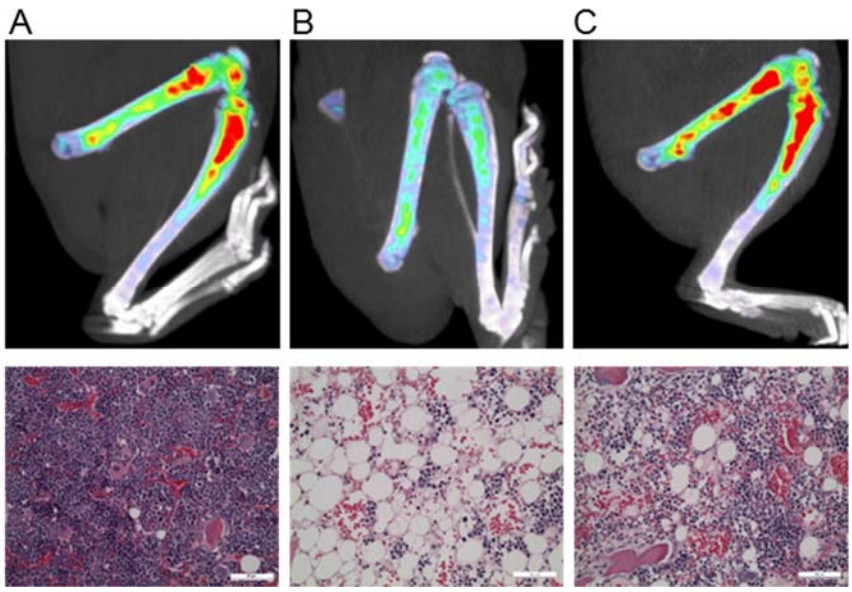

FIGURE 3. Proliferation drastically decreases immediately after radiation exposure. PET/CT (top) and hematoxylin and eosin (bottom) images of (A) sham irradiated leg and half body shielding at (B) 2 days and (C) 10 days post irradiation.

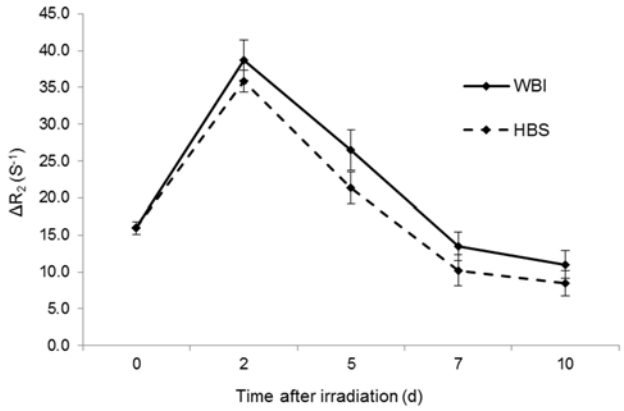

FIGURE 4. Radiation induced damage to blood-bone marrow barrier and microvascular network showing increased hemorrhaging, as measured with USPIO-MRI. Average changes in relaxation rate, ΔR_2, of whole body irradiated or half body shielded rats at 2, 5, 7, and 10 days post irradiation. WBI: whole body irradiated; HBS: half body shielding

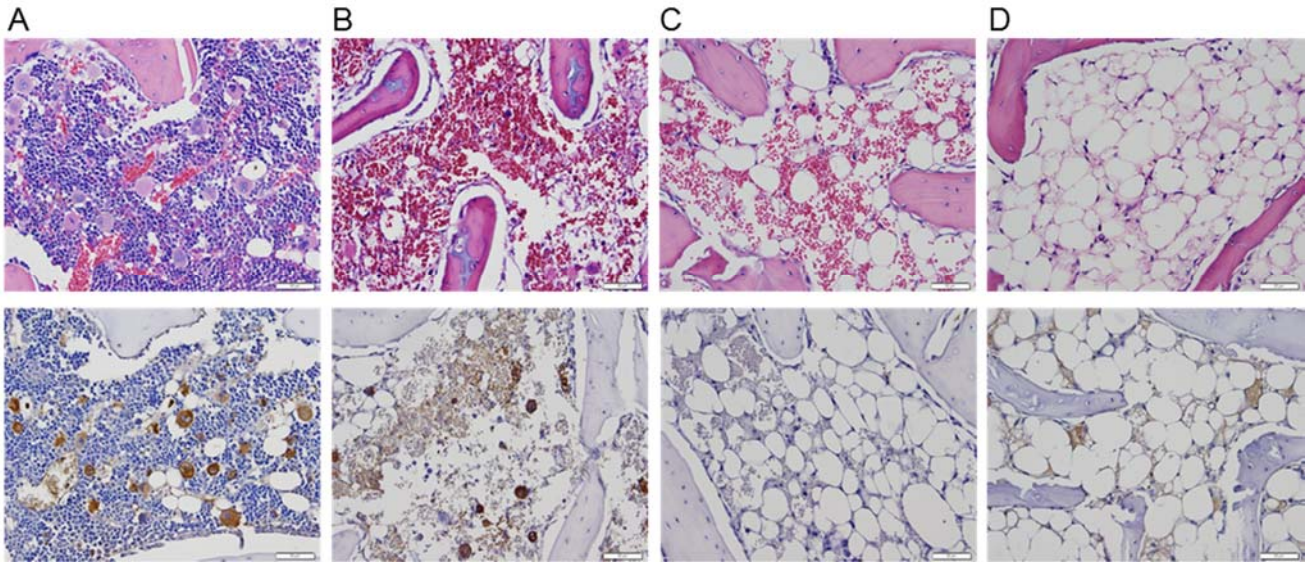

FIGURE 5. Immunohistochemical evidence of radiation-induced vascular damage. Representative images of spines stained for hematoxylin and eosin (top) and Factor VIII (bottom; brown hue) at (A) sham (B) 2 days (C) 7 days and (D) 10 days post whole body irradiation.

TABLE 1

Distribution of Bone Marrow in Sham Rats

	Volume (mL)	Total Volume (%)	Average SUV	Aggregate SUV	Total SUV (%)
Skull	2.432 ± 0.057	24.97	0.442 ± 0.020	8976.79 ± 468.003	13.21
Arms/hands/shoulders	1.335 ± 0.046	13.71	0.813 ± 0.040	9033.61 ± 486.207	13.30
Sternum	0.123 ± 0.006	1.26	1.307 ± 0.102	1327.54 ± 91.795	1.95
Backbone	2.093 ± 0.091	21.49	0.968 ± 0.049	16887.17 ± 1105.654	24.86
Hips	0.710 ± 0.039	7.29	1.282 ± 0.062	7562.37 ± 483.099	11.13
Femurs	0.807 ± 0.038	8.28	1.383 ± 0.084	9275.22 ± 651.042	13.65
Tibias	0.834 ± 0.036	8.56	1.144 ± 0.074	7946.37 ± 618.990	11.70
Whole body	9.741 ± 0.364	100.00	0.838 ± 0.042	67929.80 ± 3978.957	100.00

*Values do not include the tail

†SD

‡ n = 6

TABLE 2

Histological scoring of hemorrhage

Blood cell extravasation scores	**Sham**	**Day 2**	**Day 7**	**Day 10**
%N(0)	66.7	0	0	33.3
%N(1)	33.3	0	33.3	66.7
%N(2)	0	33.3	66.7	0
%N(3)	0	66.7	0	0
N	3	3	3	3